Shape, Shell, and Vacuole Formation during the Drying of a Single Concentrated Whey Protein Droplet

ARTICLE *in* LANGMUIR · NOVEMBER 2013

Impact Factor: 4.46 · DOI: 10.1021/la404108v · Source: PubMed

7 AUTHORS, INCLUDING:

Hervé Tabuteau
Université de Rennes 1
42 PUBLICATIONS **646** CITATIONS
SEE PROFILE

Cécile Le Floch-Fouéré
Agrocampus Ouest
38 PUBLICATIONS **64** CITATIONS
SEE PROFILE

Romain Jeantet
Agrocampus Ouest
115 PUBLICATIONS **768** CITATIONS
SEE PROFILE

Langmuir

Article

pubs.acs.org/Langmuir

Shape, Shell, and Vacuole Formation during the Drying of a Single Concentrated Whey Protein Droplet

Céline Sadek,[†,‡,§] Hervé Tabuteau,[∥] Pierre Schuck,[‡,§] Yannick Fallourd,[†] Nicolas Pradeau,[†] Cécile Le Floch-Fouéré,*[,‡,§] and Romain Jeantet[‡,§]

[†]United Pharmaceuticals, F-75000 Paris, France

[‡]INRA, UMR1253, F-35000 Rennes, France

[§]Agrocampus Ouest, UMR1253, F-35000 Rennes, France

[∥]CNRS, UMR6251, F-35000 Rennes, France

ABSTRACT: The drying of milk concentrate droplets usually leads to specific particle morphology influencing their properties and their functionality. Understanding how the final shape of the particle is formed therefore represents a key issue for industrial applications. In this study, a new approach to the investigation of droplet−particle conversion is proposed. A single droplet of concentrated globular proteins extracted from milk was deposited onto a hydrophobic substrate and placed in a dry environment. Complementary methods (high-speed camera, confocal microscopy, and microbalance) were used to record the drying behavior of the concentrated protein droplets. Our results showed that whatever the initial concentration, particle formation included three dynamic stages clearly defined by the loss of mass and the evolution of the internal and external shapes of the droplet. A new and reproducible particle shape was related in this study. It was observed after drying a smooth, hemispherical cap-shaped particle, including a uniform protein shell and the nucleation of an internal vacuole. The particle morphology was strongly influenced by the drying environment, the contact angle, and the initial protein concentration, all of which governed the duration of the droplet shrinkage, the degree of buckling, and the shell thickness. These results are discussed in terms of specific protein behaviors in forming a predictable and a characteristic particle shape. The way the shell is formed may be the starting point in shaping particle distortion and thus represents a potential means of tuning the particle morphology.

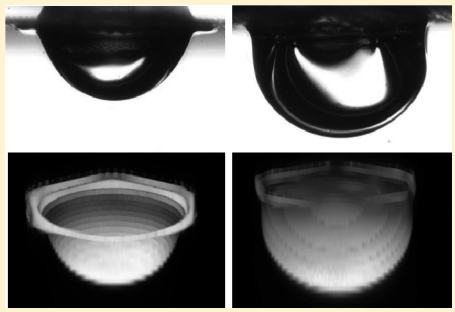

INTRODUCTION

The drying of droplets is a common process that results in dried particles with specific internal and external structures. According to the processing conditions and bulk physicochemical properties, the stress induced by spray drying may result in a wide range of particle structures such as puffed, hollow, fully filled, and buckled particles.[1−4] The final morphology determines some of the quality attributes of the particle (particle size, particle density, brittleness, dispersibility, and moisture content) and governs its end use.[2,5,6] Controlling the particle structure therefore represents a key point for several applications such as electronics,[7] optical materials,[8] drug carriers, and food powders.[9,10] However, the process of particle formation is still not fully understood and represents an extensive research field.[11] Because the evaporation of a droplet occurs within a few seconds in a spray-drying process,[12] its investigation remains difficult. One strategy is to study the drying phenomenon of a single droplet under relevant conditions. The desiccation of a single droplet deposited onto a hydrophobic substrate may in fact provide fundamental insights into particle formation.[13,14] This experimental approach allows direct and accurate observation of the droplet−particle conversion. Various physical phenomena such as solvent diffusion,[15] internal flows,[16] phase transition,[17] and skin formation are involved in the drying of a sessile droplet.[18,19] Under the given desiccation conditions (temperature, relative humidity, and pressure), the evaporation flux concentrates solutes on the free surface, and a sol−gel or glass transition may take place, thus forming a thin viscoelastic layer.[20] For highly concentrated systems (>10 wt %), this thin layer has mechanical properties that influence the shape dynamics of the droplet in a way that strongly depends on the nature of the system being investigated (colloids, polymers, or complex systems). To the best of our knowledge, only a few groups have studied the desiccation of simple biological fluids such as protein isolate dispersions.[21−27] Most of these studies have been carried out under mild drying conditions (at ambient temperature and relative humidity) with glass slides as the substrate (low contact angle). Only two studies have applied stressful drying conditions to the droplet by using hot air,[13] pressure, and relative humidity.[28] Nevertheless, understanding the behavior of proteins in stressful environments and the consequences for the structural and mechanical evolution of the

Received: June 7, 2013
Published: November 21, 2013

medium is becoming an important focus of interest in many fields.[29,30]

In this study, we focused on whey protein isolate (WPI) concentrate. WPI consists of globular proteins extracted from milk that are commonly used for nutritional, pharmaceutical, and cosmetic applications. Our aim was to investigate the shape dynamics and final structure of a whey protein droplet under stressful drying conditions on a nonwetting surface by using a hydrophobic substrate and low relative humidity. We developed an approach combining complementary methods including a microbalance, a high-speed camera, and confocal microscopy to increase our understanding of the particle-formation process under relevant conditions. It was thus possible to monitor in situ both the drying kinetics and visualization of the external and internal structures of the droplet during drying.

EXPERIMENTAL METHODS

Solution Preparation. Whey proteins represent the globular protein fraction of milk that remains soluble over the whole pH range. Whey protein isolates (WPI) are mostly composed of two globular milk proteins: 70% β-lactoglobulin, often in dimer form (molecular mass of 36.6 kg·mol^{-1}) with tertiary structure highly sensitive to temperature and pH, and 20% α-lactalbumin (molecular mass of 14.2 kg·mol^{-1}).[31] In general, it is considered that the diameters of whey proteins range between 3 and 12 nm.

In this study, the WPI concentrate was prepared from WPI industrial concentrate concentrated to 250 g·L^{-1} and diluted to 200, 150, and 100 g·L^{-1} in deionized water containing 0.02% sodium azide as a bacteriostatic agent. Proteins were labeled with fluorochrome fluorescein isothiocyanate (FITC, Sigma-Aldrich) by adding 12.5 ppm of fluorescein solution (5 g·L^{-1} FITC in dimethyl sulfoxide, DMSO, Sigma-Aldrich) to the WPI concentrate before the experiment.

Hydrophobic Substrate and Drying Conditions. A droplet of 0.42 ± 0.01 mg was formed with a microsyringe (0.5 μL syringe, SGE Analytical Science) and deposited onto a hydrophobic substrate (Figure 1). The latter was patterned with cylindrical pillars (20 μm diameter, 10 μm high) made of poly(dimethylsiloxane) (PDMS) positioned in a triangular lattice and separated from each other by a 50 μm center-to-center distance. This pattern was made according to soft lithography techniques,[32,33] and its design conferred a small contact area with the droplet, making it possible to maintain the spherical shape of the droplet and to limit its impact on droplet dynamics during drying. The substrate provided a contact angle of around 106° for a water droplet and around 103° for a WPI concentrate droplet. A pendant configuration of the droplet was adopted in order to maintain a spherical shape as much as possible and avoid an inversion of the curvature of the particle.[34] In the sessile configuration, it is well known that the shell collapses under a gravity and pressure gradient when water evaporates through the porous shell.[34,35] Therefore, with a suspended system, the impact of drying kinetics and matter might be more noticeable. Temperature, T, was kept constant at 20 °C (±0.5) whereas the relative humidity, RH, was decreased to 2% by means of excess zeolites (HG2-DES-3, Rotronic) in order to ensure a constant drying stress. It is worth noting that emphasizing that the environment around the droplet is a key factor in the drying process because the diffusion of vapor into the surrounding air is driven by the difference between the saturation pressure and the vapor pressure.[36] Thus, the drier the surrounding air, the faster the evaporation of the solvent in order to balance the vapor pressure.

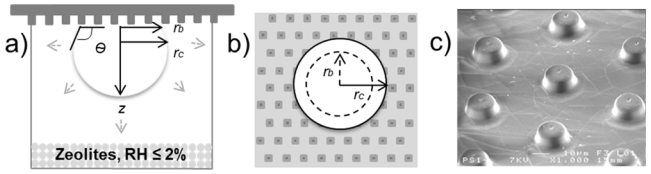

Figure 1. Schematic illustration of the experimental setup in (a) a profile view, (b) a lower view of the droplet, and (c) a scanning electron microscopy image of the cylindrical pillars (20 μm diameter, 10 μm height). The droplet is characterized by the contact angle, θ, the base radius, r_b, the cap radius, r_c and, the height, z.

Coupling Methods. The droplet−particle conversion was followed by monitoring the mass loss, the external shape, and the internal structure of the droplet under the same experimental drying conditions. (a) The mass loss, m, was tracked using an ultra-microbalance (XP2U, Mettler Toledo) with an accuracy of 0.1 μg. It is in fact a more accurate estimator of the drying kinetics than the radius or height as usually used in the literature. (b) The external shape was recorded with a high-speed camera (Fastcam MC2 10000 NB, Photron) equipped with suitable objectives (Zoom 6000, Navitar). The droplet profile was obtained by image analysis. A light (Phlox 100/100°LLUB, Stemmer imaging) illuminated the droplet from behind to produce a uniform background. The atmospheric disturbance was reduced by using a sealed glass chamber (measuring 80 × 80 × 80 mm^3). The evolution of the droplet profile was measured by means of three shape indicators: the height, z, the base radius, r_b (the radius at the contact line with the substrate), and the cap radius, r_c, of the droplet (Figure 1a,b). The cap radius represents the radius of a horizontal section of the droplet taken 60 μm from the substrate (Figure 1b). This last indicator was chosen in order to follow the shape of the droplet during drying. (c) The internal structure was studied with an inverted TE2000-E microscope. It was used in fluorescence mode with a Nikon C1 Si laser scanning imaging system and a helium−neon laser. A Nikon 10× air-immersion objective with a 0.45 numerical aperture was used. FITC was excited at 488 nm, and the fluorescence from the solution was detected at 515 nm. The evolution of the internal structure was characterized by imaging the fluorescence profile of a horizontal section of the droplet taken 60 μm from the substrate. The fluorescence in the center of the horizontal section was recorded to evaluate the internal organization.

Drying took around 10 min, and data were recorded automatically every 10 s. Experiments were repeated three times. Controls consisted of the drying of water droplets under the same experimental conditions. For water, it was considered that evaporation was diffusion-controlled. Images from the camera and the confocal microscope were analyzed with ImageJ software (U.S. National Institutes of Health). To gain a better understanding of the hydrophobic support and the final particle shape, scanning electron microscopy (SEM) has been used as a complement to the confocal microscope. The samples and the substrate were coated with gold/palladium and viewed with SEM (model 6301, JEOL) at 7 kV.

RESULTS AND DISCUSSION

Shape Dynamics during Drying. The drying kinetics of WPI at 100 g·L^{-1} are summarized in Figure 2 through dimensionless values of shape and mass descriptors as well the fluorescence intensity of a central point (Figure 2a), photographic sequences (Figure 2b), and confocal sections (Figure 2c). We identified three different stages of drying corresponding to distinct morphological events and all occurring at characteristic times: droplet buckling and vacuole formation occurred at two characteristic different times, t_B and t_V, respectively (Figure 2a).

Homogeneous Shrinkage of Droplet. When $t < t_B$ (4.2 min, Figure 2a), the spherical droplet ($\theta \approx 106°$) progressively shrank with a considerable decrease in height. The droplet decreased in volume while retaining its hemispherical shape with a constant base radius. In the early stages, the base radius was pinned, as was previously observed for protein suspension as a result of the adsorption of proteins to pillars.[23,26] The contact angle decreased continuously with time, leading to a constant contact radius evaporation mode during the first

dx.doi.org/10.1021/la404108v | Langmuir 2013, 29, 15606−15613

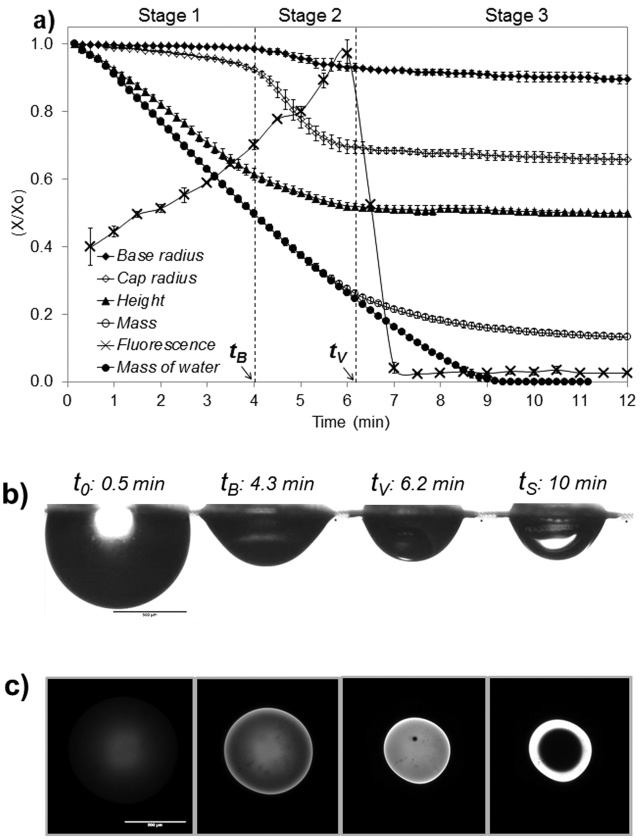

Figure 2. Droplet drying dynamics: (a) representation of dimensionless values (X/X_0) for the base radius (◆), cap radius (◇), height (▲), mass (○), fluorescence intensity (×), and pure water droplet mass (●). (b) Corresponding image sequences. (c) Confocal sections taken at z stack = 60 μm. The reference bar is 500 μm.

stage.[37] After reaching an initial equilibrium point (with a lower rate of kinetics due to the temporarily water-saturated atmosphere), the mass decreased progressively with time. The WPI droplet mass and pure water droplet mass ran almost parallel. Moreover, it was noted at this stage that the evolution of mass$^{2/3}$ was linear with time.[38] Thus, the homogeneous shrinking of the droplet before t_B could be attributed to the diffusion-controlled evaporation of water from the droplet surface into the surrounding air.

Occurrence of Buckling Instability. The second stage ($t_B < t < t_V$) was marked by a sudden change in all shape indicators as a result of the development of two types of surface instability (i.e., skin formation and its buckling). The height reduction slowed down while the cap radius decreased rapidly (Figure 2a). These two simultaneous events revealed the occurrence of the buckling instability at t_B,which is defined as the time when the slope of the cap radius curve changes significantly (Figure 2a). Confocal sections fully confirmed the strong and isotropic decrease in the cap radius (Figure 2c). As the buckling developed near the contact line, a foot appeared at the periphery of the droplet base and fixed its contact angle (Figure 2b). Near t_B, the mass loss rate did not change too much and fitted well with pure water evaporation; in contrast, the evaporation kinetics were slightly slower near t_V. All of these results revealed that significant rheological changes occurred at the surface of the droplet. It is well known for polymer and colloidal suspensions that distortions of droplets such as buckling can be explained by skin formation on the free surface.[17] These results suggest that when the skin appeared its porous properties did not initially impede the solvent diffusion through the surface, but it is likely that the thickening of the skin tended to hinder evaporation progressively.[40] The occurrence of a "gelled foot" has often been reported as a localized sol−gel transition taking place at the droplet rim and moving to the center as a gelled front.[22,39] However, we observed here that the buckling instability induced both the foot formation and fixed the height. It was therefore considered that the sol−gel transition appeared not only at the contact line but over the entire free surface of the droplet to form the droplet shell. The latter thickened with time, in accordance with the slowing down of the drying kinetics. The porous shell then bent under the internal (skin) and external constraints (substrate and difference in pressure) accumulated at the base of the droplet. It is also interesting that there was an inversion of the evaporation mode that is typical of a complex fluid. Indeed, Brutin et al.[24] reported different dynamics of the contact radius for whole blood droplets. The contact radius remained constant at the beginning of evaporation and receded or dewetted at the end. This was directly linked to the wetting properties of the substrate and the drying environment governing the gelation kinetics.

Vacuole Formation. When $t > t_V$, shape indicators no longer evolved. At t_V, confocal sections showed the rapid formation of an internal vacuole, which rapidly (around 7 min; Figure 2a) filled the entire space beneath the shell. As reported by Arai and Doi,[40] the formation of the skin is a necessary condition for vacuole initiation, as explained by a pressure change between the liquid and the atmosphere. It is possible that air enters the droplet at the same time that water diffuses through the whole shell. At around 10 min, the mass stopped evolving significantly. The shell no longer thickened under drying stress: confocal sections revealed a shell protein of 78 μm at a distance of 60 μm from the substrate (Figure 2c). Then a purely mechanical evolution of the shell occurred, leading to the development of a clear central fissure splitting the particle into two equal parts. This occurred after 30 min and with an irregular time distribution.

From the combined methods, the drying process of the WPI droplet revealed three stages involving different evaporation rates and droplet dynamics. During the first stage, the droplet behaved as a pure liquid with a faster evaporation rate. During the second stage, the protein concentration resulted in strong rheological modifications with skin formation on the free surface. Finally, the skin thickened and became a porous shell, with a sudden decrease in the evaporation rate in the last stage. In this study, stressful drying conditions strongly impacted the drying kinetics, with fast rheological changes in the medium revealing two major morphological events at t_B and t_V. Buckling has been fully investigated in the case of the evaporation of polymer and colloidal suspensions.[41] However, the formation of an internal vacuole has not been investigated in the literature, and only a few studies related the observation of hollow particles after drying, especially for lysozyme droplets.[21,42] This phenomenon may be directly linked to the stresses induced by the drying rate and skin formation. Indeed, with less stressful drying conditions at 40% RH (results not shown), the dried particle did not show an internal vacuole. Similar results were reported by Caddock and Hull,[43] who noted the influence of a dry environment on the radial solute distribution. They reported that under drier conditions the final pattern showed a large and solid peripheral deposit with a central depression

dx.doi.org/10.1021/la404108v | *Langmuir* 2013, 29, 15606−15613

whereas gelation occurred through the entire space inside the droplet under more humid conditions.

Moreover, the onset of these morphological events was also validated for higher concentrations of 150, 200, and 250 g·L^{-1} (Table 1 and Figure 3e). The characteristic time for the buckling event and thus skin formation seemed to be dictated by the initial concentration of the droplet. Indeed, t_B was observed at around 2.3 min for 200 g·L^{-1}, which was half of the value observed for 100 g·L^{-1}: the higher the initial concentration, the faster the appearance of morphological events that obviously influenced the final particle shape (Figure 3e). With higher initial concentrations, the droplet did not have time to shrink progressively and became fixed early. A foot due to the buckling phenomenon was formed whatever the concentration, but buckling was reduced at 200 and 250 g·L^{-1} with a considerably greater final height compared to that at 100 g·L^{-1} (Figure 3a–d and Table 1). Here, the foot feature was probably a result of the time available for water diffusion. In other words, it depended on the duration of phase 1 and the first part of phase 2. These findings suggested that at higher concentrations the skin was strong enough earlier to bend only partially under drying stress. These results were consistent with those of Liber et al.,[44] who showed that the structure formed by a colloidal hard sphere depended on the initial concentration.

This typical particle morphology depended strictly on both the experimental conditions (RH and contact angle) and the initial concentration, which affected the time scale of each drying regime (phases 1–3). The way the skin is formed is a key point to understanding the final characteristics of the shell and thus to controlling the particle morphology. This is the subject of the following section.

Table 1. Morphological Features Observed during the Drying of a Droplet with Different WPI Concentrations

	WPI solutions (g·L^{-1})			
morphological features	100	150	200	250
$t_{B(min)}$	4.2	3	2.3	1.3
$t_{V(min)}$	6.2	4.3	3.8	3
h_{lim}/r_b	0.79	1.09	1.17	1.29

Whey Protein Particle Formation. Particle morphology is mainly governed by (i) the sol–gel transition at the air–solution interface and (ii) the progressive thickening of the skin shell and (iii) the evolution of its mechanical properties.

Final Shape Governed by the Shell Thickness. The drying of a concentrated WPI droplet resulted in a solid particle with a hemispherical cap shape. Different central cap shapes have been reported in the literature upon the drying of concentrated solutions (colloids and polymers), with either very reduced domes[41] or elongated and taller cones[45] such as a "Mexican hat". Remarkably, the drying of WPI resulted in a smooth, hemispherical cap shape for the range of concentrations tested, with a height greater than the base radius. The occurrence of secondary levels of instability taking place at the end of drying, such as invagination with polymer solutions[17,46] or shell collapse with biological fluids,[11,47] has often been reported. In this study, the cap shape remained convex throughout the drying process without an invagination instability, revealing a certain robustness of the shell. Indeed, no peripheral cracks or fracture patterns were observed at the contact line, in contrast to studies on human biological fluids containing protein elements.[36] This is all the more surprising because the occurrence of cracks and fractures is usually explained by significant stress drying.[25,43] Only a random, single central fracture that divided the droplet into two parts sometimes appeared at the end drying as a result of the continuous evolution of stresses between the shell and the substrate (Figure 4a,b). In this study, the absence of a secondary instability associated with the neat and clean aspect of the shell fracture indicated specific mechanical properties of the shell in resisting internal and external stresses. The shell thickness was measured on the final dry particle with confocal analysis for a given *z*-stack scan and by SEM for 100, 200, and 250 g·L^{-1} (Figure 4). Analysis was performed only for the cap-shaped part of the particle that began 60 μm from the substrate. Indeed, the base of the droplet including the foot and the delamination of the droplet base made analysis difficult and can be considered to be an artifact resulting from the substrate and the initial concentration. It is worth noting that the cap shape had the same thickness, with larger values when the apex of the droplet was reached (Figure 4). As shown in Figure 4, the thickness of the shell increased with the initial concentration (from 78 μm for 100 g·L^{-1} to 100 μm for 250 g·L^{-1}). A homogeneous shell was observed for 100 g·L^{-1} (Figure 4a). This uniform protein shell is not commonly observed and many studies have reported an inhomogeneous crust with thicker particles at the base and thinner or invaginated particles at the apex.[19] Indeed,

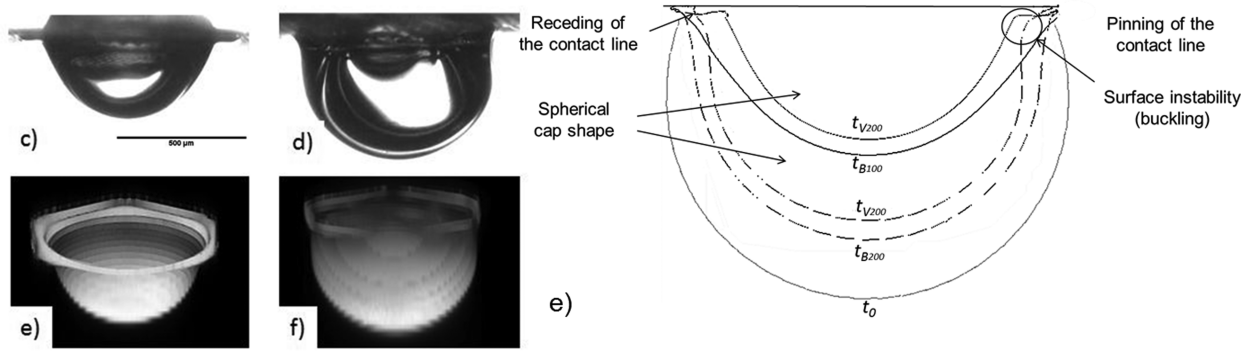

Figure 3. Images of final shapes, 3D confocal reconstitution, and profiles of droplets obtained from ImageJ analysis of 100 g·L^{-1} (a, b, e (solid line)) and 200 g·L^{-1} (c, d, e (dotted line)) WPI solutions. Droplet profiles are reported according to morphological events: buckling at t_B (noted as t_{B100} and t_{B200} for 100 and 200 g·L,$^{-1}$ respectively) and vacuole formation at t_V (noted as t_{V100} and t_{V200} for 100 and 200 g·L,$^{-1}$ respectively); t_0 is the initial droplet profile. The reference bar is 500 μm.

dx.doi.org/10.1021/la404108v | *Langmuir* 2013, 29, 15606–15613

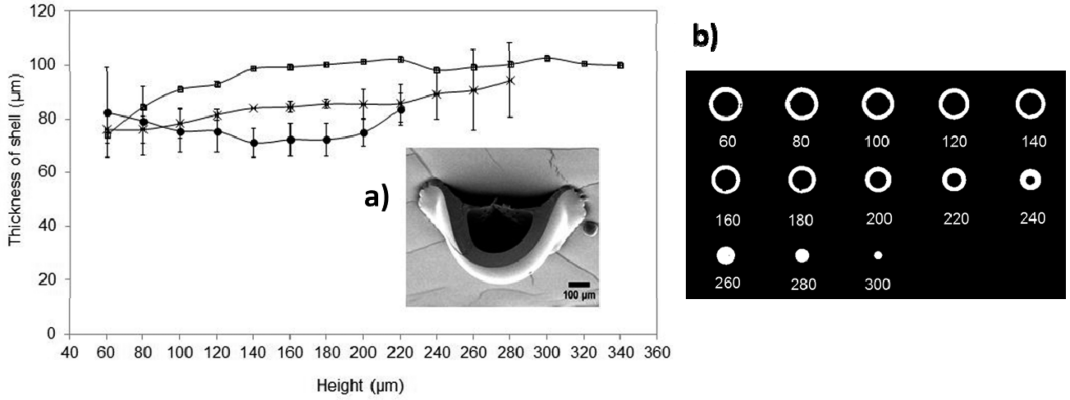

Figure 4. Shell thickness in relation to height for 100 (●), 200 (×), and 250 g·L^{-1} (■) WPI: (a) SEM image of the fracture plane of the 100 g·L^{-1} particle and (b) *z*-stack montage of a dry particle with a step of 20 μm for 100 g·L^{-1}. The shell thickness was estimated from particle sections only at relevant *z* values (i.e., above the gel foot (60 μm) and below the apex (height minus 100 μm)). Measurements were carried out only for the cap-shaped area of the dried particle ($z > 60$ μm from the substrate).

according to the droplet configuration and the drying environment, competition between internal flows may occur and result in a specific spatial distribution of solutes inside the droplet. Investigating the internal structure of the particle therefore seems to be helpful in understanding hydrodynamic flow inside the droplet during the drying process.

Skin Formation Defined by the Internal Flow Direction. During evaporation, the droplet shape is governed by competition among the Deegan flow, Marangoni flow, and evaporative flux at the droplet surface. Deegan flow is a radial outward flow driven by a higher evaporation flux at the contact line.[48] It results in an accumulation of solutes by capillarity from the center to the contact line, inducing its pinning and forming a solid deposit at the droplet periphery known as the "coffee ring". A gradient of surface tension usually involves Marangoni instability.[49] Convection rolls take place inside the droplet, dragging solutes along the surface to the center. Finally, the evaporative flux induces the diffusion of water and solutes (supposedly pulled by the water flow) from the center to the free surface to compensate for evaporated water. These three types of flow are strongly proposed in the literature to explain the distribution of solutes at the surface and skin formation.[19,50]

The importance of convection in relation to diffusion is commonly assessed through the Péclet number.[49,51] An increasing Péclet number value reveals weak diffusion movement, and the solutes are mainly driven by the flow closer to the interface and deform the heterogeneous skin, as reported by Zhang et al.[19] It may be calculated as $Pe = h_0 J/D_p$, where h_0 is the initial height of the droplet, J is the evaporation flux estimated from the loss of volume, V, per area unit, A, at the beginning of the drying process $J = -(1/A)\,dV/dt$, and D_p is the protein diffusivity estimated according to Stokes–Einstein with the protein size and viscosity of water.

In this study, *Pe* values ranged from 8 to 5 for 100 to 250 g·L,$^{-1}$ respectively. These values were very low, and we therefore considered that diffusion was the most dominant flow at the beginning of the drying process. This is in agreement with the previous discussion of the first drying phases (Figure 2a), and these finding are consistent with those of Gorr et al.[16] The authors reported a cap-shaped particle for a *Pe* of less than 0.2 and assumed that the caplike pattern dictated by the initial concentration (density) resulted from dominant diffusive transport.

The homogeneous shell revealed no spatial preference for solute accumulation and confirmed the diffusion control.[51] This assumed a progressive accumulation of solutes from the center to the surface pulled by an evaporative flux. The formation of the protein shell suggested hydric but not mechanical equilibrium in the buckling phenomenon. Indeed, we speculate a small Deegan effect due to the pinned contact line with an increase in the number of solutes at the triple contact line.

Sol–Gel Transition at a Critical Concentration. As suggested above, the skin formation may be explained by a sol–gel transition induced by a local and critical concentration of proteins. This critical concentration is considered to be reached when the viscosity increases strongly and the elastic behavior of the system becomes significant.[51] Its occurrence during the drying process may be related to the evolution of the solid mass concentration of the droplet (Figure 5). Obviously,

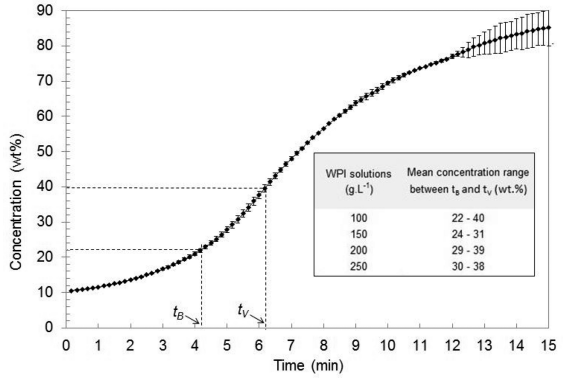

Figure 5. Representation of the average solute concentration according to the drying time scale for the 100 g·L^{-1} solution of WPI and other concentrations (inset).

under the stressful drying conditions implemented in this study, the sol–gel transition occurred locally at the interface (air–solution or substrate–solution). However, the mean concentration can provide an initial idea of the minimum value of the solid fraction required to trigger these phenomena.

A phase transition between t_B and t_V was shown previously in which the droplet became a particle, with the formation of a skin progressively thickening into a solid glassy shell. In Figure 5, it can be seen that the buckling event for the 100 g·L^{-1}

dx.doi.org/10.1021/la404108v | *Langmuir* 2013, 29, 15606–15613

solution occurred at an average concentration of 22 wt %. The still-increasing curve suggests a porous shell that is not completely dry. For the other concentrations, the buckling occurred from 24 to 30 wt %. It seemed that the average critical concentration increased with the initial concentration. This was also observed for colloidal hard spheres.[44] Moreover, the rapid occurrence of the buckling instability for WPI solutions of 200 and 250 $g{\cdot}L^{-1}$ confirmed the assumption that a transition occurred between 22 and 30 wt %.

Without a consideration of the droplet system, the behavior of globular proteins in a highly concentrated state was investigated using osmotic stress and rheological techniques. Parker et al.,[52] studied β-lactoglobulin concentrates. They observed a relative viscosity divergence and a change in viscoelasticity at around 54% w/w. The same analysis has also been performed on another protein, bovine serum albumin.[53] The authors reported that the solution behaved as a solid for concentrations of around 60%. These two studies compared the transition of the protein concentrate to the glass transition in colloidal hard spheres. Although proteins are not as spherical as colloidal hard spheres with well-defined interparticle forces, they show analogous rheological behavior in relation to high viscosity and the glassy stage.[54] On this assumption, the system is dominated by repulsive excluded volume interactions that lead to a glasslike transformation.[53] Our system was mainly dominated by charge repulsion. The sol−gel transition resulted from these phenomena and also from the fact that proteins are rapidly advected close to the shell, where they form a disordered structure within the shell.[55]

In our study, it is of note that 200 and 250 $g{\cdot}L^{-1}$ solutions quickly underwent a buckling phenomenon that suggested the sol−gel transition was close to these concentrations (i.e., around 30 wt %), which are substantially lower than the concentration range reported by Parker et al.[52] but consistent with the critical concentration for the phase transition of other biological fluids described in the literature.[56,57] Moreover, the sol−gel transition occurred first at the air droplet interface because of water evaporation; therefore, the fact that the local whey protein concentration is higher than the average concentration obtained for the overall mass balance on the entire droplet is to be expected, consistent with the concentration range reported by Parker et al.[52] Despite different experimental conditions, results regarding the phase transition and the characteristics of the shape of the final particle (formation of a cap shape without the occurrence of a secondary instability) seem to be closer to an ideal charged colloidal system under fast drying conditions and with high initial concentrations. Nevertheless, the latter is still under investigation.

CONCLUSIONS

The drying behavior of a simplified biological fluid (i.e., a whey protein concentrate in deionized water at different concentrations (100, 200, and 250 $g{\cdot}L^{-1}$)) was investigated in this study. An innovative and reproducible particle was obtained through selected drying conditions and devices. This smooth, hemispherical, hollow particle was investigated with complementary methods in order to describe the transformation of the droplet in a dried particle in situ and ex situ.

The drying of the WPI droplet revealed three regimes involving different evaporation rates and droplet dynamics, all resulting from various physical mechanisms. At the beginning, the droplet behaved as a pure liquid without a significant influence of the protein surface activity. Next, a sol−gel transition was believed to occur for an average concentration of between 22 and 30 wt %. The gelation fixed the surface area while the water was still evaporating, inducing the buckling of the droplet and revealing a hydric rather than a mechanical equilibrium (diffusion) occurring with the initial surface instability. The skin then progressively thickened into a homogeneous protein shell, leading to the formation of an internal vacuole. The final particle remained a smooth and hemispherical cap shape, with the degree of buckling at the droplet base depending on the initial concentration. It was clear that the initial concentration of the solution influenced the mechanical stability of the shell and thus the final shape of the particle. This particular morphology depended on the drying rate, the contact angle, the time of water diffusion (influenced by the initial concentration), and the nature of the solutes, in this case whey proteins. Controlling a particular design as a spherical cap shape from protein solutions is becoming a point of interest in research for solving many applications such as encapsulation in biological, biomedical, and pharmaceuticals fields.

AUTHOR INFORMATION

Corresponding Author

*E-mail: cecile.lefloch@agrocampus-ouest.fr

Notes

The authors declare no competing financial interest.

ACKNOWLEDGMENTS

We thank United Pharmaceuticals for funding this work and for the many fruitful discussions. We thank M. N. Madec for her help with confocal microscopy and the UMR ESE for lending us the microbalance. We thank Loic Joanny for the scanning electron microscopy observations.

REFERENCES

(1) Werner, S. R. L.; Edmonds, R. L.; Jones, J. R.; Bronlund, J. E.; Paterson, A. H. J. Single droplet drying: transition from the effective diffusion model to a modified receding interface model. *Powder Technol.* **2008**, *179*, 184−189.

(2) Vehring, R.; Foss, W. R.; Lechuga-Ballesteros, D. Particle formation in spray drying. *J. Aerosol Sci.* **2007**, *38*, 728−746.

(3) Walton, D. E.; Mumford, C. J. The morphology of spray-dried particles - the effect of process variables upon the morphology of spray-dried particles. *Chem. Eng. Res. Design* **1999**, *77*, 442−460.

(4) Eslamian, M.; Ashgriz, N. Effect of precursor, ambient pressure, and temperature on the morphology, crystallinity, and decomposition of powders prepared by spray pyrolysis and drying. *Powder Technol.* **2006**, *167*, 149−159.

(5) Hassan, H. M.; Mumford, C. Mechanisms of drying of skin-forming materials; the significance of skin formation and a comparison between three types of material. *Drying Technol.* **1996**, *14*, 1763−1777.

(6) Walton, D. E.; Mumford, C. J. Spray dried products - Characterization of particle morphology. *Chem. Eng. Res. Design* **1999**, *77*, 21−38.

(7) Jung, H. J.; Huh, J.; Park, C. Kinetically driven self-assembly of a binary solute mixture with controlled phase separation via electrohydrodynamic flow of corona discharge. *Nanoscale* **2012**, *4*, 6219−6234.

(8) Iskandar, F. Nanoparticle processing for optical applications - a review. *Adv. Powder Technol.* **2009**, *20*, 283−292.

(9) Chan, H. K. Dry powder aerosol drug delivery−opportunities for colloid and surface scientists. *Colloids Surf., A* **2006**, *284−285*, 50−55.

(10) Vehring, R. Pharmaceutical particle engineering via spray drying. *Pharm. Res.* **2008**, *25*, 999−1022.

(11) Schutyser, M.; Perdana, J.; Boom, R. Single droplet drying for optimal spray drying of enzymes and probiotics. *Trends Food Sci. Technol.* **2012**, *27*, 73−82.
(12) Schuck, P.; Dolivet, A.; Mejean, S.; Zhu, P.; Blanchard, E.; Jeantet, R. Drying by desorption: a tool to determine spray drying parameters. *J. Food Eng.* **2009**, *94*, 199−204.
(13) Perdana, J. A.; Fox, M. B.; Schutyser, M. A. I.; Boom, R. M. Single-droplet experimentation on spray drying: evaporation of a sessile droplet. *Chem. Eng. Technol.* **2011**, *34*, 1151−1158.
(14) Marin, A. G.; Gelderblom, H.; Susarrey-Arce, A.; van Houselt, A.; Lefferts, L.; Gardeniers, J. G. E.; Lohse, D.; Snoeijer, J. H. Building microscopic soccer balls with evaporating colloidal fakir drops. *Proc. Natl. Acad. Sci. U.S.A.* **2012**, *109*, 16455−16458.
(15) Erbil, H. Y. Evaporation of pure liquid sessile and spherical suspended drops: a review. *Adv. Colloid Interface Sci.* **2012**, *170*, 67−86.
(16) Gorr, H. M.; Zueger, J. M.; Barnard, J. A. Characteristic size for onset of coffee-ring effect in evaporating lysozyme-water solution droplets. *J. Phys. Chem. B* **2012**, *116*, 12213−12220.
(17) Pauchard, L.; Allain, C. Buckling instability induced by polymer solution drying. *Europhys. Lett.* **2003**, *62*, 897−903.
(18) Boulogne, F.; Giorgiutti-Dauphine, F.; Pauchard, L. The buckling and invagination process during consolidation of colloidal droplets. *Soft Matter* **2013**, *9*, 750−757.
(19) Zhang, Y.; Yang, S.; Chen, L.; Evans, J. R. G. Shape changes during the drying of droplets of suspensions. *Langmuir* **2008**, *24*, 3752−3758.
(20) Okuzono, T.; Ozawa, K.; Doi, M. Simple model of skin formation caused by solvent evaporation in polymer solutions. *Phys. Rev. Lett.* **2006**, *97*, 1−4.
(21) Accardo, A.; Gentile, F.; Mecarini, F.; De Angelis, F.; Burghammer, M.; Di Fabrizio, E.; Riekel, C. In situ X-ray scattering studies of protein solution droplets drying on micro- and nano-patterned superhydrophobic PMMA surfaces. *Langmuir* **2010**, *26*, 15057−15064.
(22) Tarasevich, Y. Y.; Pravoslavnova, D. M. Segragation in desiccated sessile drops of biological fluids. *Eur. Phys. J. E* **2007**, *22*, 311−314.
(23) Annarelli, C. C.; Fornazero, J.; Bert, J.; Colombani, J. Cracks patterns in drying protein solution drops. *Eur. Phys. J. E* **2001**, *5*, 599−603.
(24) Gorr, H. M.; Zueger, J. M.; Barnard, J. A. Lysozyme pattern formation in evaporating drops. *Langmuir* **2012**, *28*, 4039−4042.
(25) Gorr, H. M.; Zueger, J. M.; McAdams, D. R.; Barnard, J. A. Salt-induced pattern formation in evaporating droplets of lysozyme solutions. *Colloids Surf., B* **2013**, *103*, 59−66.
(26) Choi, C. H.; Kim, C. J. Γ.C. Droplet evaporation of pure water and protein solution on nanostructured superhydrophobic surfaces of varying heights. *Langmuir* **2009**, *25*, 7561−7567.
(27) Accardo, A.; Burghammer, M.; Di Cola, E.; Reynolds, M.; Di Fabrizio, E.; Riekel, C. Lysozyme fibrillation induced by convective flow under quasi contact-free conditions. *Soft Matter* **2011**, *7*, 6792−6796.
(28) Baldwin, K. A.; Granjard, M.; Willmer, D. I.; Sefiane, K.; Fairhurst, D. J. Drying and deposition of poly(ethylene oxide) droplets determined by Péclet number. *Soft Matter* **2011**, 7819−7826.
(29) Bouchoux, A.; Schorr, D.; Daffé, A.; Cambert, M.; Gésan-Guiziou, G.; Mariette, F. Molecular mobility in dense protein systems: an investigation through 1H NMR relaxometry and diffusometry. *J. Phys. Chem. B* **2012**, *116*, 11744−11753.
(30) Zimmerman, S. B.; Minton, A. P. Macromolecular crowding - biochemical, biophysical, and physiological consequences. *Annu. Rev. Biophys. Biomol. Struct.* **1993**, *22*, 27−65.
(31) Walstra, P., Wouters, J. T. M., Geurts, T. J., Eds.; *Dairy Science and Technology*, 2nd ed.; CRC/Taylor & Francis: Boca Raton, FL, 2006; Chapter 2, pp 76−79.
(32) Moulinet, S.; Bartolo, D. Life and death of a fakir droplet: Impalement transitions on superhydrophobic surfaces. *Eur. Phys. J. E* **2007**, *24*, 251−260.
(33) Papadopoulos, P.; Deng, X.; Mammen, L.; Drotlef, D.-M.; Battagliarin, G.; Li, C.; Mullen, K.; Landfester, K.; del Campo, A.; Butt, H.-J.; Vollmer, D. Wetting on the microscale: shape of a liquid drop on a microstructured surface at different length scales. *Langmuir* **2012**, *28*, 8392−8398. Addition/correction for the original article. Papadopoulos, P.; Deng, X.; Mammen, L.; Drotlef, D. M.; Battagliarin, G.; Li, C.; Mullen, K.; Landfester, K.; del Campo, A.; Butt, H. J.; Vollmer, D. Wetting on the microscale: shape of a liquid drop on a microstructured surface at different length scales. *Langmuir* **2012**, *28*, 10136−10139.
(34) Chen, X. L.; Boyko, V.; Rieger, J.; Reinhold, F.; Reck, B.; Perlich, J.; Gehrke, R.; Men, Y. F. Buckling-induced structural transition during the drying of a polymeric latex droplet on a solid surface. *Soft Matter* **2012**, *8*, 12093−12098.
(35) Pauchard, L.; Couder, Y. Invagination during the collapse of an inhomogeneous spheroidal shell. *Europhys. Lett.* **2004**, *66*, 667−673.
(36) Brutin, D.; Sobac, B.; Nicloux, C. Influence of substrate nature on the evaporation of a sessile drop of blood. *J. Heat Trans.* **2012**, *134*, 1−7.
(37) Picknett, R. G.; Bexon, R. Evaporation of sessile or pendant drops in still air. *J. Colloid Interface Sci.* **1977**, *61*, 336−350.
(38) Arcamone, J.; Dujardin, E.; Rius, G.; Perez-Murano, F.; Ondarcuhu, T. Evaporation of femtoliter sessile droplets monitored with nanomechanical mass sensors. *J. Phys. Chem. B* **2007**, *111*, 13020−13027.
(39) Ma, X.; Xia, Y.; Chen, E. Q.; Mi, Y.; Wang, X.; Shi, A. C. Crust effect on multiscale pattern formations in drying micelle solution drops on solid substrates. *Langmuir* **2004**, *20*, 9520−9525.
(40) Arai, S.; Doi, M. Skin formation and bubble growth during drying process of polymer solution. *Eur. Phys. J. E* **2012**, 35.
(41) Parisse, F.; Allain, C. Drying of colloidal suspension droplets: experimental study and profile renormalization. *Langmuir* **1997**, *13*, 3598−3602.
(42) Manukyan, S.; Sauer, H. M.; Roisman, I. V.; Baldwin, K. A.; Fairhurst, D. J.; Liang, H.; Venzmer, J.; Tropea, C. Imaging internal flows in a drying sessile polymer dispersion drop using spectral radar optical coherence tomography (SR-OCT). *J. Colloid Interface Sci.* **2013**, *395*, 287−293.
(43) Caddock, B. D.; Hull, D. Influence of humidity on the cracking patterns formed during the drying of sol-gel drops. *J. Mater. Sci.* **2002**, *37*, 825−834.
(44) Liber, S. R.; Borohovich, S.; Butenko, A.; Schofield, A. B.; Sloutskin, E. Dense colloidal fluids fom denser ammorphous sediments. *Proc. Natl. Acad. Sci. U.S.A.* **2013**, *110*, 5769−5773.
(45) Pauchard, L.; Allain, C. Stable and unstable surface evolution during the drying of a polymer solution drop. *Phys. Rev. E* **2003**, *68*, 052801−1−052801−4.
(46) Tsapis, N.; Dufresne, E. R.; Sinha, S. S.; Riera, C. S.; Hutchinson, J. W.; Mahadevan, L.; Weitz, D. A. Onset of buckling in drying droplets of colloidal suspensions. *Phys. Rev. Lett.* **2005**, 94.
(47) Rogers, S.; Wu, W. D.; Lin, S. X. Q.; Chen, X. D. Particle shrinkage and morphology of milk powder made with a monodisperse spray dryer. *Biochem. Eng. J.* **2012**, *62*, 92−100.
(48) Deegan, R. D.; Bakajin, O.; Dupont, T. F.; Huber, G.; Nagel, S. R.; Witten, T. A. Capillary flow as the cause of ring stains from dried liquid drops. *Nature* **1997**, *389*, 827−829.
(49) Majumder, M.; Rendall, C. S.; Eukel, J. A.; Wang, J. Y. L.; Behabtu, N.; Pint, C. L.; Liu, T. Y.; Orbaek, A. W.; Mirri, F.; Nam, J.; Barron, A. R.; Hauge, R. H.; Schmid, H. K.; Pasquali, M. Overcoming the "coffee-stain" effect by compositional Marangoni-flow-assisted drop-drying. *J. Phys. Chem. B* **2012**, *116*, 6536−6542.
(50) Maki, K. L.; Kumar, S. Fast evaporation of spreading droplets of colloidal suspensions. *Langmuir* **2011**, *27*, 11347−11363.
(51) Okuzono, T.; obayashi, M.; Doi, M. Final shape of a drying thin film. *Phys. Rev. E* **2009**, *80*, 1−11.
(52) Parker, R.; Noel, T. R.; Brownsey, G. J.; Laos, K.; Ring, S. G. The nonequilibrium phase and glass transition behavior of ß-lactoglobulin. *Biophys. J.* **2005**, *89*, 1227−1236.

(53) Brownsey, G. J.; Noel, T. R.; Parker, R.; Ring, S. G. The glass transition behavior of the globular protein bovine serum albumin. *Biophys. J.* **2003**, *85*, 3943−3950.
(54) Loveday, S. M.; Creamer, L. K.; Singh, H.; Rao, M. A. Phase and rheological behavior of high-concentration colloidal hard-sphere and protein dispersions. *J. Food Sci.* **2007**, *72*, 101−107.
(55) Marin, A. G.; Gelderblom, H.; Lohse, D.; Snoeijer, J. H. Order-to-disorder transition in ring-shaped colloidal stains. *Phys. Rev. Lett.* **2011**, *107*, 085502.
(56) Sobac, B.; Brutin, D. Structural and evaporative evolutions in desiccating sessile drops of blood. *Phys. Rev. E: Stat., Nonlinear, Soft Matter Phys.* **2011**, *84*, 1−5.
(57) Bouchoux, A.; Debbou, B.; Gesan-Guiziou, G.; Famelart, M. H.; Doublier, J. L.; Cabane, B. Rheology and phase behavior of dense casein micelle dispersions. *J. Chem. Phys.* **2009**, *131*, 165106-1−165106-11.